

Enriched haloes at redshift $z = 2$ with no star-formation: Implications for accretion and wind scenarios^{*}

N. Bouché^{1,2,3}, M. T. Murphy⁴, C. Péroux⁵, T. Contini^{2,3}, C. L. Martin¹, N. M. Forster Schreiber⁶, R. Genzel⁶, D. Lutz⁶, S. Gillessen⁶, L. Tacconi⁶, R. Davies⁶, F. Eisenhauer⁶

¹*Department of Physics, University of California, Santa Barbara, CA 93106, USA; Marie Curie Fellow*

²*CNRS; Institut de Recherche en Astrophysique et Planétologie [IRAP] de Toulouse, 14 Avenue E. Belin, F-31400 Toulouse, France*

³*Université Paul Sabatier de Toulouse; UPS-OMP; IRAP; F-31400 Toulouse, France*

⁴*Swinburne University of Technology, Mail H30, PO Box 218, Hawthorn, Victoria 3122, Australia*

⁵*Observatoire d'Astrophysique de Marseille-Provence, 38 rue Frédéric Joliot-Curie, F-13388 Marseille, France*

⁶*Max Planck Institut für extraterrestrische Physik, Giessenbachstraße, D-85748 Garching, Germany*

Accepted 22 Jul 2011— Received 17 Jan 2011

ABSTRACT

In order to understand which process (e.g. galactic winds, cold accretion) is responsible for the cool ($T \sim 10^4$ K) halo gas around galaxies, we embarked on a program to study the star-formation properties of galaxies selected by their Mg II absorption signature in quasar spectra. Specifically, we searched for the H α line emission from galaxies near very strong $z \simeq 2$ Mg II absorbers (with rest-frame equivalent width $W_r^{\lambda 2796} \gtrsim 2 \text{ \AA}$) because these could be the signposts of outflows or inflows. Surprisingly, we detect H α from only 4 hosts out of 20 sight-lines (and 2 out of the 19 H I-selected sight-lines), despite reaching a star-formation rate (SFR) sensitivity limit of $2.9 M_\odot \text{ yr}^{-1} (5\sigma)$ for a Chabrier initial mass function. This low success rate (4/20) is in contrast with our $z \simeq 1$ survey where we detected 66% (14/21) of the Mg II hosts (down to $0.6 M_\odot \text{ yr}^{-1}$, 5σ). Taking into account the difference in sensitivity between the two surveys, we should have been able to detect ≥ 11.4 (≥ 7.6) of the 20 $z \simeq 2$ hosts—assuming that SFR evolves as $\propto (1+z)^\gamma$ with $\gamma = 2.5$ (or $\gamma = 0$) respectively—whereas we found only 4 galaxies. Interestingly, all the $z = 2$ detected hosts have observed SFRs $\gtrsim 9 M_\odot \text{ yr}^{-1}$, well above our sensitivity limit, while at $z = 1$ they all have $\text{SFR} < 9 M_\odot \text{ yr}^{-1}$, an evolution that is in good agreement with the evolution of the SFR main sequence, i.e. with $\gamma = 2.5$. Moreover, we show that the $z = 2$ undetected hosts are not hidden under the quasar continuum after stacking our data. They also cannot be outside our surveyed area as this latter option runs against our sample selection criteria ($W_r^{\lambda 2796} > 2 \text{ \AA}$) and the known $W_r^{\lambda 2796}$ –impact parameter relation for low-ionization ions. Hence, strong Mg II absorbers could trace star-formation driven winds in low-mass halos ($M_h \leq 10^{10.6} M_\odot$) provided that the winds do not extend beyond 20 kpc in order not to violate the evolution of the absorber number density $dN/dz(\text{Mg II})$. Alternatively, our results imply that $z = 2$ galaxies traced by strong Mg II absorbers do not form stars at a rate expected ($3\text{--}10 M_\odot \text{ yr}^{-1}$) for their (halo or stellar) masses, supporting the existence of a transition in accretion efficiency at $M_h \simeq 10^{11} M_\odot$. This scenario can explain both the detections and the non-detections.

Key words: galaxies: evolution, galaxies: formation, galaxies: high-redshifts, galaxies: haloes, intergalactic medium, quasars: absorption lines

1 INTRODUCTION

The current paradigm for cold dark matter (CDM) (White & Rees 1978) is now well grounded in, for instance, the many galaxy clustering surveys (Madgwick & et al., 2003; Budavári & et al., 2003; Eisenstein & et al., 2005). As a result, the growth rate of dark matter haloes is well determined thanks to various large-scale dark mat-

^{*} Based on observations made with ESO Telescopes at Paranal Observatories under program ID 060.A-9041, 076.A-0527, 079.A-0341, 079.A-0600, 081.A-0568.A, 081.A-0682, 082.A-0580.

ter numerical simulations (e.g. Springel et al. 2006). For instance, in the Millennium simulation, the growth rate is determined to be

$$\dot{M}_h \propto M_h^s (1+z)^t, \quad (1)$$

with $t \sim 2.2$ and a mass index s greater than unity $s \simeq 1.15$ (Birnboim et al. 2007; Neistein & Dekel 2008; Genel et al. 2008; McBride et al. 2009). The index s is greater than unity because the index of the initial dark matter (DM) power spectrum $n \sim 0.8$ is less than unity (Neistein et al. 2006; Birnboim et al. 2007). Hence, this growth rate is very generic and follows from the initial dark matter (DM) power spectrum.

In contrast, our understanding of galaxy growth is more limited and is certainly incomplete. The G-dwarf problem (van den Bergh 1962; Schmidt 1963) and other chemical arguments (e.g. Larson 1974) show that gas accretion must have been an important factor in building present day galaxies. In addition, theoreticians keep pointing out that in haloes where the cooling time is short (compared to the dynamical time), the accretion efficiency of ‘cold’ ($T \sim 10^4$ K) baryons must be high (e.g. White & Frenk 1991). This mode of ‘cold accretion’ is well defined in haloes with mass less than the shock mass $M_{\text{sh}} \sim 10^{12} M_\odot$ where the cold gas is not shock-heated to the virial temperature (Birnboim & Dekel 2003; Kereš et al. 2005, 2009; van de Voort et al. 2011), and can also take place in haloes more massive than this limit at $z > 2$ due to geometrical effects (streams) (Ocvirk et al. 2008; Dekel et al. 2009).

While streams—with gas columns ranging from $10^{19.5} \text{cm}^{-2}$ to $10^{21.5} \text{cm}^{-2}$ according to Dekel et al. (2009)—are expected to have small ($< 5\%$) covering fractions (e.g. Faucher-Giguère & Kereš 2011; Kimm et al. 2011), the covering fraction of ‘cold accretion gas’ with columns $N_{\text{HI}} > 10^{18} \text{cm}^{-2}$ can be higher ($\sim 20\%$) in galaxies below M_{sh} according to Stewart et al. (2011). It is therefore important to study the gaseous haloes of galaxies, which can be detected only in absorption in the spectra of distant background quasars (QSOs).

For instance, the low ionization Mg II doublet ($\lambda\lambda 2796, 2803 \text{\AA}$) is of great interest because it traces gas at $T \sim 10^4$ K over a wide range of redshifts $0.1 \leq z \leq 2.5$ and over a wide range of hydrogen column densities $10^{16} \leq N_{\text{HI}} \leq 10^{22} \text{cm}^{-2}$ (Churchill et al. 2000). The large range of physical parameters may thus trace the inter-stellar medium of a host (e.g. Prochaska & Wolfe 1997), parts of outflows (e.g. Nulsen et al. 1998; Schaye 2001), and/or $T \sim 10^4$ K gas related to accretion (e.g. Kacprzak et al. 2010; Stewart et al. 2011).

However, the sub-class of strong Mg II absorbers with rest-frame equivalent widths (rest-EW or $W_r^{\lambda 2796}$) above $\sim 1-2 \text{\AA}$ are particularly interesting as they are the signposts of a collection of clouds spanning large velocity widths $\Delta v > 100 \text{km s}^{-1}$ (Ellison 2006). At low and intermediate redshifts, the physical connection between strong Mg II absorbers and star-forming galaxies has been established since the early nineties (Lanzetta & Bowen 1990; Bergeron & Boissé 1991; Bergeron et al. 1992; Steidel & Sargent 1992). Thanks to the advances in large sky surveys such as SDSS (e.g. Abazajian & et al., 2003; Abazajian et al. 2009), this connection is further supported by various statistical/stacking analyses (e.g. Bouché et al. 2006; Zibetti et al. 2007; Ménard et al. 2011). Bouché et al. (2006) showed that $z \sim 0.6$ Mg II clouds are not virialized, a result interpreted as supporting evidence that

supernova-driven winds are the dominant sources of strong Mg II with $W_r^{\lambda 2796} > 2 \text{\AA}$ ¹.

Direct evidence for this scenario comes from our $z = 1$ SINFONI Survey For Line Emitters (z1SIMPLE) (Bouché et al. 2007), where we targeted two dozen QSO fields with known Mg II absorbers with $W_r^{\lambda 2796} > 2 \text{\AA}$ and successfully unveiled the H α signature of the host in 14 out of 21 of the cases. These star-forming (SF) galaxies were found to have observed star-formation rates (SFR) of about $\sim 1-10 M_\odot \text{yr}^{-1}$, corresponding to a mean dust-corrected SFR of $\sim 10 M_\odot \text{yr}^{-1}$. This experiment further strengthens the connection between SF galaxies and strong Mg II absorbers with $W_r^{\lambda 2796} > 2 \text{\AA}$.

Additional supporting evidence for this interpretation comes from a variety of studies. For instance, Bond et al. (2001) showed that, in a few systems with $W_r^{\lambda 2796} > 1.8 \text{\AA}$, the high-resolution profile of the low-ion Mg II shows clear signatures of a wind super-bubble. Similarly, the study of 2 ultra-strong (with $W_r^{\lambda 2796} \gtrsim 3 \text{\AA}$) Mg II absorbers of Nestor et al. (2011) showed that star-burst driven outflows are necessary to account for the velocity extent of the absorption and that each field contains a starburst (with bright [O II], H β emission lines). Using large data sets of 5000 and 8500 absorbers respectively, Noterdaeme et al. (2010) and Ménard et al. (2011) found a clear correlation between $W_r^{\lambda 2796}$ and [O II] luminosity in the stacked spectra of Mg II absorbers. These results favor outflows as the mechanism responsible for strong Mg II absorption, and as a consequence, they link intervening Mg II absorbers with the blue-shifted Mg II absorptions seen in the spectra of star forming galaxies (e.g. Martin & Bouché 2009; Weiner et al. 2009; Rubin et al. 2010).

Given the successes of our z1SIMPLE survey and the paucity of H I absorbers identified at $z \sim 2$ (only 5 have been identified by Lowenthal et al. 1991; Djorgovski et al. 1996; Möller et al. 2004; Heinmüller et al. 2006; Fynbo et al. 2010)², we embarked on a program designed to detect the hosts of 18 strong Mg II and 7 H I absorbers at $z \simeq 2$. This paper presents the results of this $z \sim 2$ survey. Throughout, we use a standard ‘737’ cosmology, i.e. we use a $h = 0.7$, $\Omega_M = 0.3$, $\Omega_\Lambda = 0.7$ cosmology.

2 SAMPLE SELECTION AND DATA REDUCTION

2.1 Sample selection

The main goal of this survey is to extend the $z \sim 1$ SIMPLE survey of Bouché et al. (2007) to $z \simeq 2$ absorbers using the K -band of the Spectrograph for INtegral Field Observations in the Near Infrared (SINFONI). We therefore selected sight-lines from the SDSS data base (DR5) and the 2dF Quasar Redshift survey (2QZ) data bases as in Bouché et al. (2007) with the criterion $W_r^{\lambda 2796} > 2 \text{\AA}$. This criterion was used for the following two reasons. First, in the super-wind scenario, as argued in our z1SIMPLE survey, the strongest absorbers (as measured by $W_r^{\lambda 2796}$) ought to have the largest star-formation rates, hence the largest H α fluxes. Second, the $W_r^{\lambda 2796} > 2 \text{\AA}$ criterion empirically selects the hosts with the smallest impact parameters (ρ) with $\rho < 35 h^{-1} \text{kpc}$ (e.g. Steidel 1995). At $z \sim 1$ and $z \sim 2$, this corresponds to $\sim 4''$, which means that the host-galaxy will fall within the searched area ($10'' \times 10''$) limited by the SINFONI field of view ($7.5'' \times 7.5''$). From the pool

¹ see Tinker & Chen (2008) for an alternative interpretation.

² Recently, Fynbo et al. (2011) reported another detection of a $z = 2.58$ DLA, which we view as being tentative given its very low signal-to-noise.

of ~ 100 strong $z \sim 2$ Mg II absorbers available in SDSS, we were able to observe 18 Mg II absorbers with appropriate coordinates and favorable redshifts (see Table 1), i.e. whose corresponding H α emission line would not be affected by the sky OH emission lines.

Our observations also include 7 $z \sim 2$ H I absorbers (see Table 1) selected from having H I column densities $\log N_{\text{H I}}(\text{cm}^{-2}) \gtrsim 20.0$ mostly from Prochaska et al. (2005). These 7 SINFONI fields include 2 from archival Science Verification data (Q0216+08 and Q2243-60). To increase the number of H I absorbers, we will include 12 other $z = 2$ damped Ly α absorbers (DLAs) observed with SINFONI from the sample of Péroux et al. (2011a)³ and Péroux et al. (2011b).

Some of the targets meet both the Mg II and the H I criteria (SDSSJ1316, SDSSJ2059-05, Q2222-09, Q2243-60) and were included a posteriori if they were not in the original sample. In total, our Mg II sample is made of 20 sight-lines, and the H I sample is made of 19 sight-lines (see section 3).

2.2 Observational Strategies

The observations presented here were carried out with the near-IR integral field spectrometer (IFU) SINFONI (Eisenhauer & et al. 2003; Bonnet et al. 2004) mounted at the Cassegrain focus of the VLT UT4 telescope. The near-IR IFU contains a set of mirror slicers that splits the focal plane in 32 parallel slitlets and rearranges them in a pseudo long-slit fed into the spectrometer part of the instrument. These reflective slicers are at the core of the high-throughput of this instrument.

In total, we have obtained K -band SINFONI observations towards 28 $z \simeq 2$ absorbing galaxies listed in Table 1 using the $0.125''$ pixel scale. These observations were taken during the 2006-2009 period and started during SINFONI guaranteed time observing (GTO) runs. Subsequently, the observations for this program were obtained during the observing runs 081.A-0682 and 082.A-0580 under good observing conditions with near-IR full-width at half-maximum of $\text{FWHM} \simeq 0.6''$.

Our $z = 2$ SINFONI survey for line emitters (z2SIMPLE) is made of the fields selected according to the criterion described in § 2.1 (Table 1). Even though SINFONI is more sensitive in the K -band than in the J -band by 20%, we integrated on each field for about 2hr, i.e. longer by a factor of $\sim 2\times$ compared to the 40min integrations used in Bouché et al. (2007) in order to account for the luminosity distance increase from $z = 1$ to $z = 2$.

Despite the field of view being $7.5'' \times 7.5''$, we optimized the searched area by adopting a ‘on source’ dithering strategy resulting in contiguous surveyed area of $10'' \times 10''$. The central region is thus observed four times per observing block made of $4 \times 600\text{s}$.

2.3 Data Reduction

The data reduction was performed as in Förster Schreiber et al. (2009), i.e. using the MPE SINFONI pipeline (SPRED, Schreiber et al. 2004; Abuter et al. 2006) complemented with additional custom routines to optimize the reduction for faint high-redshift targets such as the OH sky line removal scheme of Davies (2007). The steps are outlined here. Firstly, after creating the dark frames and flat-field frames, we optimized the bad pixel identification from these frames, as artifacts and residual bad pixels could

lead to spurious sources, and we applied these to the data. Secondly, in order to further improve the cosmic ray removal, we used the Laplacian edge cosmic ray removal technique of van Dokkum (2001). Bad pixels and cosmic rays were replaced by interpolation onto the neighboring 2D pixels on the detectors. Thirdly, arc lamp frames were used to generate the ‘wavemap’ by tracing the edges and curvature of the slitlets. Because slight wavelength shifts may occur, the wavemaps were cross-calibrated against the known vacuum wavelengths of the sky OH emission lines. These were found in the first 600s exposure taken per field, which was used as a reference frame. Then, the pre-processed science data frames were reconstructed into cubes, corrected for distortion using the tuned wavemaps. Given that we are looking for emission lines, the atmospheric correction was turned off in order to avoid an additional interpolation.

Given that SINFONI is a Cassegrain instrument, small spectral shifts occur during the observations ($< 0.2\text{pixels}$). In order to ensure excellent sky-subtraction, we corrected these shifts by cross-correlating each of the science frames spectrally against the reference frame (the first science exposure). At this stage the data cubes still contain the sky background. We used the algorithm of Davies (2007) to subtract the sky background pair-wise and optimize the OH subtraction. The algorithm involves scaling each group of telluric OH lines separately. We applied the heliocentric correction to the sky-subtracted frames.

For each observing block, we use the continuum of the quasar to spatially register the various sets of observations. Finally, a co-added cube is obtained from the average of all the individual sky-subtracted 600s exposures using a median clipping at 2.5σ .

The data of the standard stars were reduced in a similar way as the science data and intrinsic stellar absorption lines were removed according to their spectral type. The flux calibration of the data was performed on a night-by-night basis using the broadband magnitudes of the standards from 2MASS. The flux calibration is accurate to $\sim 15\%$. Finally, the atmospheric transmission was calibrated out by dividing the science cubes by the integrated spectrum of the telluric standard.

3 RESULTS

3.1 Low Detection Rate

The mean depth of our survey is determined in two independent ways. First, we measure the pixel noise in a region that is within $2''$ of the QSO and at the wavelength of the expected H α line. We scale the noise per pixel to a region corresponding to an unresolved source of $0.8''$ (FWHM), i.e. over 32 spatial and 8 spectral pixels to compute our 5σ flux limit⁴: $\sim 1.8 \times 10^{-17} \text{ erg s}^{-1} \text{ cm}^{-2}$.

Second, we inserted fake sources with known fluxes, assuming a Gaussian profile with a FWHM of $0.8''$, into our datacubes at the wavelength of the expected H α line. We attempted to detect the source and determined the flux level where the source is no longer visible. This technique gives similar values, i.e. $\sim 2.0 \times 10^{-17} \text{ erg s}^{-1} \text{ cm}^{-2}$, and is akin to a 95% completeness limit.

The flux limits for each field are listed in Table 2, and on average, our flux limit allows us to detect star-forming galaxies with SFRs greater than $> 2.9 M_{\odot} \text{ yr}^{-1}$ —uncorrected for dust and assuming a Chabrier (2003) initial mass function

³ We excluded Q0405-331 which is an associated systems with $z_{\text{abs}} \simeq z_{\text{qso}}$.

⁴ We include the correction for correlated noise as in Förster Schreiber et al. (2009), namely $\sigma_{\text{real}} \sim 2 \times \sqrt{N_{\text{pix}}} \sigma_{\text{pix}}$.

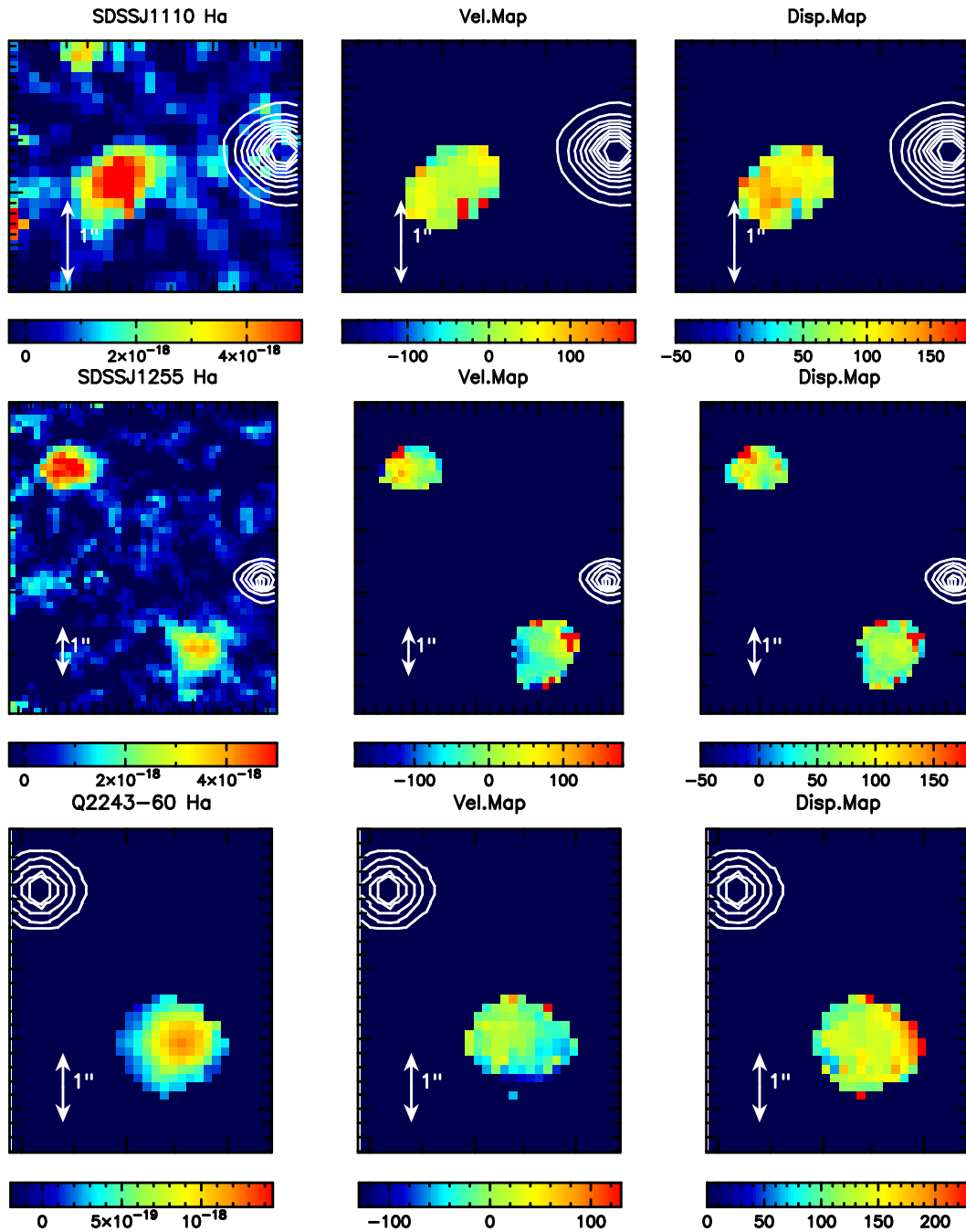


Figure 1. Flux ($\text{erg s}^{-1} \text{cm}^{-2}$), velocity (km s^{-1}) and dispersion (km s^{-1}) maps towards SDSSJ1110+0244 (a), SDSSJ1255+0305 (b) and Q2243-60 (c). In each panel, the contours show the location of the quasar.

(IMF). Despite our ability to detect star-forming galaxies with $\text{SFR}(5\sigma) \geq 2.9 M_{\odot} \text{yr}^{-1}$, we have detected H α from very few galaxies. Out of our SINFONI observations towards 18 Mg II absorbers, we detect H α emission of only 3 galaxies (towards SDSSJ111008.61+024458.0, SDSSJ125525.67+030518.4 and Q2243-60). Towards SDSSJ1255+0305, we found 2 H α galaxies within 40km s^{-1} of the absorber redshift $z = 2.1144$, and we attribute the one with the smallest impact parameter to the Mg II absorber. Towards SDSSJ1144+0959, we detected the continuum of a galaxy 19 kpc away, however we are unable to determine its redshift.

Including the 2 sight-lines from Péroux et al. (2011b) that

meet our Mg II criteria a posteriori, namely SDSSJ2059-05 and SDSSJ2222-09, our global detection rate is 4/20 since the host towards SDSSJ2222-09 was also detected by Péroux et al. (see also Fynbo et al. 2010). This detection rate (4/20) is in sharp contrast with our z1SIMPLE survey, where we detected two thirds (14/21) of the host galaxies (Bouché et al. 2007). We return to the significance of the low detection rate in section 3.3.

3.2 Notes on the detected fields

Figure 1(a-c) shows the flux, velocity and dispersion maps of the 3 fields (SDSSJ111008.61+024458.0, SDSSJ125525.67+030518.4 and Q2243–60, respectively) towards which we could detect the host. The host of the absorber towards SDSSJ111008.61+024458.0 is found only 17kpc North from the QSO. The absorber at $z = 2.1187$ has $W_r^{\lambda 2796} = 2.97 \pm 0.17 \text{ \AA}$ (Murphy & Liske 2004; Prochaska et al. 2005) and is found to have a SFR = $9.1 M_\odot \text{ yr}^{-1}$ for a Chabrier IMF, corresponding to a dust-corrected SFR₀ of $\sim 19 M_\odot \text{ yr}^{-1}$. Its velocity field is indicative of a merger system with a reversal of the velocity field, hence we refrain ourselves in assigning a dynamical mass. The average dispersion of $\sigma \sim 120 \text{ km s}^{-1}$.

The host of the absorber towards SDSSJ125525.67+030518.4 with $W_r^{\lambda 2796} = 3.20 \pm 0.23 \text{ \AA}$ (Murphy & Liske 2004; Prochaska et al. 2005) is found at 14kpc from the QSO. The host has a SFR = $8.6 M_\odot \text{ yr}^{-1}$ calculated also assuming a Chabrier IMF, corresponding to a dust-corrected SFR₀ of $\sim 18 M_\odot \text{ yr}^{-1}$. The velocity field shows a clear rotation pattern of $v_{\max} \sin i \sim \pm 70 \text{ km s}^{-1}$ with a dispersion that peaks at $\sigma \sim 70 \text{ km s}^{-1}$ in the center. The intrinsic dispersion is $\sigma_0 \sim 30 \text{ km s}^{-1}$ in the outskirts. The dynamical mass within the half-light radius ($0.44''$) is $M_{1/2} \sim 2.0 \times 10^{10} M_\odot$, taking into account the inclination $i = 24^\circ$ estimated from the axis ratio $b/a = 0.9$. Using v_{\max} , our estimate of the haloe mass is $M_h \sim 2.5 \times 10^{11} M_\odot$.

The host towards Q2243–60 has the highest H α flux in our sample, reaching almost $\sim 1 \times 10^{-16} \text{ erg s}^{-1} \text{ cm}^{-2}$, corresponding to an observed⁵ SFR = $18 M_\odot \text{ yr}^{-1}$. The velocity field also shows a rotation pattern with a large central dispersion $\sim 120 \text{ km s}^{-1}$. This galaxy is less resolved (its half-light radius $\sim 0.5''$ is similar to the PSF $\sim 0.6''$). We recently obtained SINFONI observations (in H and K) with adaptive optics (AO) for this field that will be presented elsewhere (Bouché et al. in preparation). We can already report that the velocity field is resolved with $v_{\max} \sin i \simeq 100 \text{ km s}^{-1}$, the intrinsic dispersion is $\sigma_0 \sim 100 \text{ km s}^{-1}$. With an inclination of $57 \pm 2^\circ$, the dynamical mass within the half-light radius ($0.45''$) is $M_{1/2} \sim 1.8 \times 10^{10} M_\odot$. The halo mass is estimated at $M_h \sim 2 \times 10^{11} M_\odot$ from v_{\max} .

This absorber has a large Mg II rest-frame equivalent width $W_r^{\lambda 2796} = 2.6 \text{ \AA}$ corresponding to a velocity width of $\sim 250 \text{ km s}^{-1}$ (Ellison 2006). This DLA was discovered by the Hamburg/ESO QSO Survey (Reimers & Wisotzki 1997). Its H I column density is $\log[N_{\text{HI}}/\text{cm}^{-2}] = 20.7$. Lopez et al. (2002) presented a deep (28ksec) UVES spectra of this QSO with S/N ranging from > 50 to 80. These observations show that this DLA has an absorption metallicity that is $[\text{Zn}/\text{H}] = -1.10 \pm 0.05$, close to the iron abundance $[\text{Fe}/\text{H}] = -1.26 \pm 0.02$, indicating a low dust depletion.

3.3 How many detections are expected?

Before interpreting this apparent low detection rate (4/20), we need to be certain (i) that the sample properties are similar and (ii) that our $z = 1$ sources could have been detected at $z = 2$. On the first point, a KS-test for the $W_r^{\lambda 2796}$ distributions gives a probability of $P = 0.93$, showing that the two distributions are very consistent with each other. In other words, the low success rate cannot be attributed to differences in our sample selection. We also

⁵ Using H α /H β , we find, in Bouché et al. (in preparation), that $E(B - V) \sim 0.6$ and therefore the dust-corrected SFR is SFR₀ of $\sim 77 M_\odot \text{ yr}^{-1}$.

found no differences in the doublet ratio ($\text{DR} = W_r^{2803}/W_r^{2796}$), nor in Mg I rest-EW distributions. However, we note that the parent $z = 2$ sample made of 75 absorbers with $W_r^{\lambda 2796} \gtrsim 2 \text{ \AA}$ has a Fe II 2600 \AA /Mg II 2796 \AA ratio that is lower than the parent $z = 1$ sample by 30% (0.4 vs. 0.6).

We now quantify whether the galaxies in our z1SIMPLE survey could have been detected at $z = 2$. While the answer to this question depends directly on the flux limit of our survey, it also depends on the assumed evolution of the SFR properties from $z = 1$ to $z = 2$.

For the sensitivity aspect, our z2SIMPLE survey is more sensitive ($\sim 1.8 \times 10^{-17} \text{ erg s}^{-1} \text{ cm}^{-2}$) than our z1SIMPLE survey ($2.6 \times 10^{-17} \text{ erg s}^{-1} \text{ cm}^{-2}$ computed over the same ‘volume’ of pixels), thanks to the increased throughput in K and longer exposure times. In spite of better flux limits, our $z = 2$ SFR limit—computed for a Chabrier IMF—is $2.9 M_\odot \text{ yr}^{-1}$ (not corrected for dust), i.e. $\sim 5 \times$ worse than at $z = 1$ ($0.6 M_\odot \text{ yr}^{-1}$, not corrected for dust)⁶ given the increase in luminosity distance ($D_L \propto (1+z)^2$). See Table 2 for the individual limits taking into account the redshift dependent noise.

From the cumulative SFR distribution of the $z = 1$ SIMPLE survey (Bouché et al. 2007) shown in Figure 2, we see that 6 of the 14 $z = 1$ detected galaxies would not have been detected at $z = 2$ given our survey completeness limit (vertical dashed line). Similarly, using 10,000 Monte Carlo resamplings, we find that 99% of the time 6 galaxies would not be detected if the SFR distributions were the same at both epochs. However, the SFR distribution for the detected hosts is very different at the two epochs as Figure 2 shows. At $z = 2$, all the detections have $\text{SFR} \gtrsim 9 M_\odot \text{ yr}^{-1}$, while none have such high SFRs in the $z = 1$ survey. Thus, if the SFRs evolve strongly, as suggested by the three detected hosts in Figure 2 and by the evolution of the SFR–Mass sequence, which evolves as $\propto (1+z)^{2.5}$ (see Eq. 3 below), then only 2 of the 14 $z = 1$ hosts would not have been detected. Therefore, we expect a detection or ‘success’ rate of $\hat{p} = 0.38$ (8/21), assuming no evolution of the SFR distribution, and of $\hat{p} = 0.57$ (12/21) assuming a SFR evolution going as $\propto (1+z)^{2.5}$.

Hence, we ought to find ≥ 7.6 or ≥ 11.4 hosts depending on the assumed SFR(z) evolution, whereas 4 galaxies were found. Treating the individual fields as independent experiments with a success rate given by p , the number of success follows a binomial distribution (Cameron 2011). The probability to have only 4 successes from such a binomial distribution is 0.045(0.0007), i.e. the $z = 2$ detection rate is different than the $z = 1$ detection rate at 2.0σ or 3.4σ assuming SFR(z) goes as $\propto (1+z)^\gamma$ with $\gamma = 0$ or $\gamma = 2.5$, respectively (see table 3).

3.4 Closing loopholes

Before interpreting these results, we ask the following questions: (i) can the hosts be outside the SINFONI field of view? (ii) can the H α host emission be hidden under the QSO continuum?

(A) Are the $z = 2$ hosts outside the field of view? By design, both the $z = 1$ and this $z = 2$ sample were selected to have rest- $W_r^{\lambda 2796} > 2 \text{ \AA}$. This criteria corresponds to a maximum impact parameter $\rho_{\max} \sim 35 \text{ kpc}$ given the well-known anti-correlation between $W_r^{\lambda 2796}$ and impact parameter (e.g. Lanzetta & Bowen 1990; Steidel et al. 1995; Chen et al. 2010) for $z \sim 1$ systems and was chosen to ensure that the host would fall within our mapping

⁶ Note in Bouché et al. (2007), we quoted dust-corrected $3-\sigma$ limits.

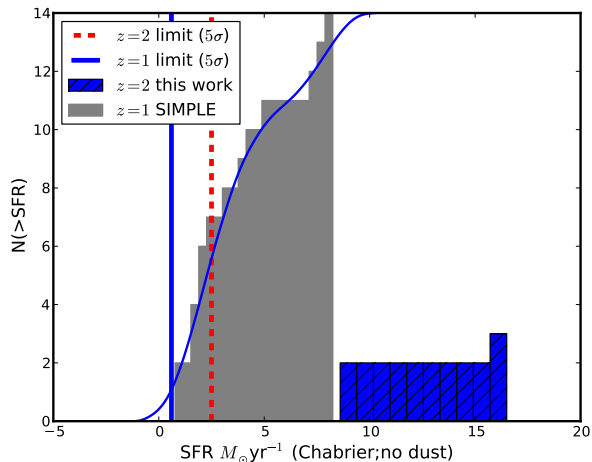


Figure 2. Cumulative observed SFR distributions. The curve shows the smoothed distribution. The grey (hatched) histogram shows the $z = 1$ ($z = 2$) distribution, respectively. At high-redshifts, all the detections have $\text{SFR} \gtrsim 9 M_{\odot} \text{ yr}^{-1}$, while none have such high SFRs in the $z = 1$ survey. The detection limits are indicated as vertical lines and show that at most 6 of the 14 $z = 1$ galaxies would not have been detected in this survey (assuming no evolution).

region ($\sim 10'' \times 10''$ or $80 \text{ kpc} \times 80 \text{ kpc}$). The normalization of the $W_r^{\lambda 2796-\rho}$ anti-correlation may expand between the two epochs. However, as the Universe was denser at $z = 2$, it is difficult to imagine that the normalization actually expanded. Not only this would be opposite to the galaxy and halo size evolution, but it would also contradict the observations of Chen et al. (2010) and Steidel et al. (2010). Chen et al. (2010) showed that the scatter in the Mg II EW- ρ anti-correlation scales with stellar mass $\propto M_{\star}^{0.28}$ (and weakly on sSFR). In other words, our results would imply the opposite, namely that the scatter scales inversely proportional to M_{\star} . Similarly, Steidel et al. (2010) showed that the averaged rest-EW of another low-ion (Si II with similar ionization potential as Mg II) is also anti-correlated with impact parameter. They found that the (average) rest-EW of Si II1526 is much less than $\lesssim 0.3 \text{ \AA}$ at impact parameters $\gtrsim 40 \text{ kpc}$. We have stacked our SDSS spectra and found that on average the non-detections have a rest-EW $\sim 0.8 \text{ \AA}$ for Si II1526. In other words, in conjunction with the Steidel et al. (2010) results, our sample of $> 2 \text{ \AA}$ Mg II absorbers has no properties consistent with being outside our mapping region.

(B) Are the $z = 2$ hosts too close to the QSO? An IFU is a very good tool to untangle H α emission even with impact parameters less than the QSO point-spread-function (PSF). This is nicely demonstrated by the J0226–28 sight-line in our $z = 1$ sample (Bouché et al. 2007) where the H α emission is detected $0.25''$ from the QSO PSF (FWHM $\sim 0.8''$).

In the present survey, however, it is possible that the H α emission is hidden under the QSO continuum, i.e. within a radius of $0.3''$ from the QSO. In order to address this, we dereshifted and stacked the 16 SINFONI cubes of the non-detected subsample. The continuum-subtracted image, shown in Fig.3, reaches the same flux limits within $0.3''$ of the QSO PSF as the ones quoted in section 3.1. Therefore, we can say with confidence that we find no evidence for H α emission in the stacked SINFONI cube, ruling out the possibility that the hosts were too close to the QSO.

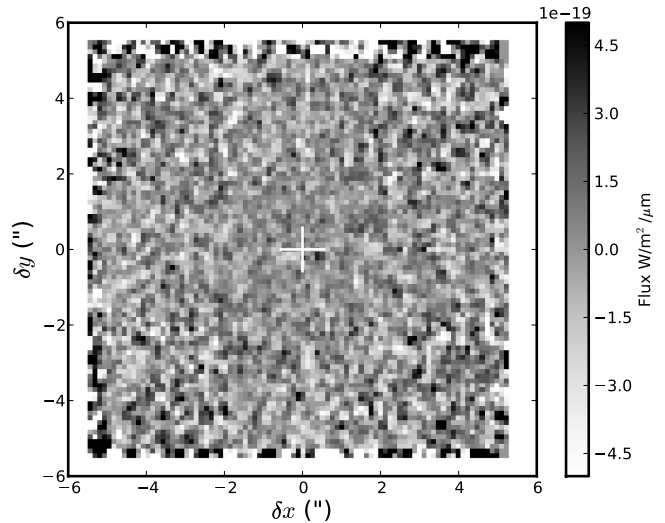


Figure 3. Continuum subtracted image of the stacked SINFONI cube extracted around H α of the 16 non-detected absorbers. The cross shows the location of the (stacked) continuum. We find no evidence for H α emission in the stacked cube down to $\sim 10^{17} \text{ erg s}^{-1} \text{ cm}^{-2}$, i.e. $\text{SFR} 1.5 \sim$, ruling out the possibility that the hosts were within $0.3''$ from the QSO.

4 IMPLICATIONS FOR THE NATURE OF Mg II SYSTEMS.

Having established that we are not limited by the QSO continuum, nor by the field of view, the low detection rate show clearly that, in the most neutral terms, the $z = 2$ Mg II population probes gaseous haloes that are different than at $z = 1$. We now attempt to constrain the meaning of ‘different’ by placing limits on the host mass assuming known scaling relations and the evolution of dN/dz .

4.1 Mass constraints from the SFR sequence.

In the mass regime where cooling times are short (i.e. where cold accretion dominates), SFR is driven by the (net) baryonic accretion rate as shown in Dekel et al. (2009); Dutton et al. (2010) and Bouché et al. (2010). The baryonic accretion rate is then simply given by the cosmological baryonic fraction f_B times the dark-matter accretion rate \dot{M}_h (Eq. 1) which is set by the cosmological parameters (e.g. Neistein et al. 2006). Hence, for a given accretion efficiency ϵ , we have

$$\text{SFR} \sim \epsilon f_B \dot{M}_h \sim 6 \epsilon_{1.0} M_{h,12}^{1.15} (1+z)^{2.25} M_{\odot} \text{ yr}^{-1}, \quad (2)$$

where $M_{h,12}$ the halo mass in units of $M_h/10^{12} M_{\odot}$ and we use $\epsilon_{1.0} \equiv \epsilon/1.0$ since Genel et al. (2008) (see also Dekel et al. 2009; Bouché et al. 2010) showed that the accretion efficiency ϵ must be in the 70-80% range in order to account for the large SFRs of $z = 2$ star-forming galaxies⁷. This equation allows us to put limits on the halo mass of the hosts, but before applying it to our survey, we demonstrate its validity on several galaxy samples.

⁷ Our assumption of $\epsilon = 1.0$ is not – as it may seem – extreme. Indeed, a lower and more realistic efficiency would be compensated by the more appropriate net SFR, which is $\sim 1/2 \times \text{SFR}$ if SN outflow rates are proportional to SFRs. Hence, $1/2 \text{SFR} \sim \epsilon_{0.5} f_b \dot{M}_h$, which is equivalent to equation 2.

The expected SFRs determined from Eq. 2 agree well with the observed SFRs at a given halo mass for a wide variety of galaxies. For instance, Lyman break galaxies (LBGs), which have halo masses $\sim 10^{11.8} M_\odot$ from their clustering (Adelberger et al. 2005) or from their rotation curves (Förster Schreiber et al. 2006), have an expected SFR in the range of $30\text{--}100 M_\odot \text{ yr}^{-1}$, which is in good agreement with the observed values for $z = 2$ star-forming galaxies (e.g. Förster Schreiber et al. 2009; Erb et al. 2006). Similarly, the $z = 1$ Mg II absorbers with $W_r^{\lambda 2796} > 2 \text{ \AA}$ reside in haloes with $M_h \sim \times 10^{11.3 \pm 0.4} M_\odot$, as several clustering analyses (e.g. Bouché et al. 2006; Gauthier et al. 2009; Lundgren et al. 2009) have shown, and are expected to have SFRs in the range $\text{few--}10 M_\odot \text{ yr}^{-1}$, in very good agreement with the observed SFR distribution shown in Fig. 2.

Now that we have validated Eq. 2, we turn it around using our SFR upper limit to put limits on the halo mass of our $z = 2$ non-detected sample. Our limit of $\text{SFR} < 2.9 M_\odot \text{ yr}^{-1}$ corresponds to low mass haloes with masses $M_h \lesssim 4 \times 10^{10} M_\odot$ ($V_h \sim 65 \text{ km s}^{-1}$). Similarly, the SFR– M_\star relationship (e.g. Elbaz et al. 2007; Daddi et al. 2007; Drory & Alvarez 2008; Santini et al. 2009; Pannella et al. 2009; Damen et al. 2009; Karim et al. 2011) can be used to place a limit on the stellar mass M_\star . These results show that the SFR– M_\star sequence is

$$\text{SFR} \sim 150 M_{\star 11}^{0.8} (1+z)^{2.7}, \quad (3)$$

where $M_{\star 11} \equiv M_\star / 10^{11} M_\odot$ and $(1+z)_{3.2} \equiv (1+z)/3.2$. Our limit of $\text{SFR} \lesssim 2.9 M_\odot \text{ yr}^{-1}$ corresponds to $M_\star \simeq 6 \times 10^8 M_\odot$ if we extrapolated the SFR–sequence to low masses. Note, this stellar mass agrees well with the limit on the halo mass we just placed and is thus not an independent result. Indeed, these numbers would place such a host along the low-mass end of the known M_\star – M_h relation (Shankar et al. 2006; van den Bosch et al. 2007; Guo et al. 2010; Moster et al. 2010; Behroozi et al. 2010).

In summary, the host of strong Mg II absorbers could in principle be in very low mass haloes with $M_h \lesssim 4 \times 10^{10} M_\odot$, i.e. below our SFR limit⁸. In the next section, we ask whether this low-mass conclusion is consistent with the observed evolution of dN/dz .

4.2 Constraints from dN/dz .

The number of absorbers per unit redshift dN/dz is a well measured quantity (e.g. Nestor et al. 2005; Prochter et al. 2006). A more appropriate quantity in our context is the number of absorbers per unit co-moving distance dN/dX and these surveys have shown that dN/dX does not evolve from $z = 1$ and $z = 2$. The number of absorbers per unit co-moving distance, dN/dX , for $z = 1$ absorbers is:

$$\frac{dN}{dX}(> 2\text{\AA}; z = 1) \equiv 0.02 \frac{n_{11.3}}{10^{-2}} \left(\frac{R}{35 \text{ kpc}} \right)^2, \quad (4)$$

where n is the halo number density, $\sigma = \pi R^2$ is the physical cross-section and $n_{11.3} \equiv M_h / 10^{11.3}$ in Eq. 4.

Because $n(M_h, z)$, the co-moving density of haloes, is a very weak function of z from $z = 0$ up to $z = 5$ (Mo & White 2002), we can say that any evolution of the absorber cross-section will

imply an evolution of the typical halo mass M_h via:

$$\frac{dN}{dX}(> 2\text{\AA}; z) \equiv 0.02 \frac{n_{11.3}}{10^{-2}} \left(\frac{R}{35 \text{ kpc}} \right)^2 \left(\frac{1+z}{1.8} \right)^{-2m}, \quad (5)$$

for any index m of the evolution of the cross-section. The physical cross-section of galaxies (and haloes) are indeed smaller at higher redshifts as demonstrated by the numerous groups (e.g. Dahlen et al. 2007; Williams et al. 2010; Mosleh et al. 2011). These surveys indicate that the size evolution index m in Eq. 5 is ~ 1 .

For such an index $m = 1$, the redshift factor in Eq. 5 is then about $0.3 = [(1+2.2)/(1+0.8)]^{-2}$, which means that the density of halo $n(M_h)$ must be higher by a factor $3 \times$ in order to account for the constant dN/dX . In the previous section, we have established that the hosts of our Mg II sample might be in very low-mass galaxies, with halo masses $M_h \lesssim 4 \times 10^{10} M_\odot$. Such low-mass haloes are more numerous by a factor of ~ 4 (e.g. Mo & White 2002). Therefore, the cross-section evolution could compensate for the higher number density of low-mass haloes provided that the cross-section evolves.

4.3 Implications for the nature of Mg II absorbers

In order to account for our low success rate, in the last section we discussed two possibilities, namely the $z = 2$ hosts could reside (i) in haloes with similar masses to those at $z = 1$ ($M_h \sim 10^{11.3} M_\odot$), or (ii) in haloes with very low masses ($M_h \sim 10^{10.6} M_\odot$) below our flux limit. The first option violates our observations because such haloes are expected to have SFRs $> 10 M_\odot \text{ yr}^{-1}$ from the SFR– M_\star or SFR– M_h sequence, whereas we find only 3 such galaxies down to $2.9 M_\odot \text{ yr}^{-1}$.

4.3.1 Wind scenario

The second option is equivalent to a scenario invoking winds in low mass galaxies. In such a scenario, the large equivalent widths of Mg II are the signature of ‘cold’ gas ($T \sim 10^4 \text{ K}$) entrained in outflows at a few hundreds of km s^{-1} . This option would explain our low detection rate but –as we showed– it is not consistent with the observed number density of absorbers, dN/dX , unless the cross-section of absorbers has evolved strongly as $\propto (1+z)^{-1}$. Given that the $z = 1$ cross-section of strong Mg II absorbers is typically $\rho \sim 35\text{--}40 \text{ kpc}$ (e.g. Steidel et al. 1995; Bouché et al. 2006), the cross-section of $z = 2$ absorbers cannot then be larger than 20 kpc.

Hence, our results are consistent with the outflow scenario as argued by others (Bond et al. 2001; Bouché et al. 2006, 2007; Nestor et al. 2011), provided that the $z = 2$ hosts reside in halos less massive than $M_h \sim 10^{10.6} M_\odot$ and that the extent of the wind traced by $W_r^{\lambda 2796} > 2\text{\AA}$ is not larger than 20 kpc ($\sim 2.5''$). A consequence of this scenario is that the outflow ‘efficiency’ (defined as $W_r^{\lambda 2796}/\text{SFR}$, i.e. more clouds (larger $W_r^{\lambda 2796}$) per unit SFR are being produced at $z = 2$ than at $z = 1$) was much larger at $z = 2$ than at $z = 1$. However, this scenario cannot explain the few galaxies that we do detect. Indeed, because the SFRs are higher at $z = 2$ than at $z = 1$, this $W_r^{\lambda 2796}$ -to-SFR ratio is then lower at $z = 2$, not higher. Thus, the wind scenario alone cannot explain the detections and non-detections at the same time.

In Fig. 4, we put our $z = 2$ results in a more global context. The solid lines show the averaged evolution of halos with time $M_h(z)$ and the dashed lines show the predicted SFR ($\sim \epsilon f_B \dot{M}_h$) given by Eq. 2 for a maximum accretion efficiency $\epsilon = 1.0$.

⁸ Note that despite having a narrow range of $W_r^{\lambda 2796}$, the range of halo mass could be larger. Such a scatter is enough to explain our few detections.

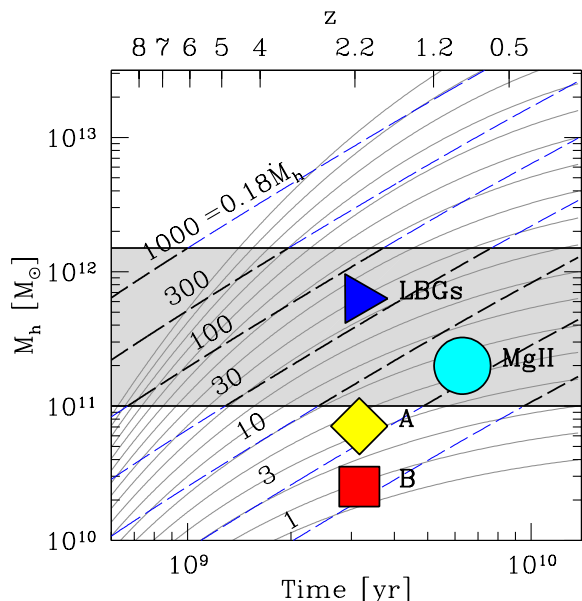


Figure 4. Each solid curve represents a halo growth history $M_h(z)$. The cosmological (baryonic) growth rate, namely $M\epsilon f_B \dot{M}_h$ where f_B is the baryonic fraction, is shown by the dashed lines. These dashed lines can be used as a proxy for SFR when (cold) accretion is efficient with $\epsilon \simeq 1.0$ (e.g. Genel et al. 2008), i.e. below the shock mass $M_{\text{sh}} 10^{12} M_\odot$, and possibly only in the grey band according to Bouché et al. (2010) and Cantalupo (2010). For illustration purposes, the inferred SFRs for LBGs (triangle) and strong $z \sim 1$ Mg II absorbers (circle) are in very good agreement with the observed SFRs (see text). Strong $z = 2$ Mg II absorbers could be caused either in galaxies with low accretion efficiency (scenario A) or in low mass SF galaxies below our SFR limit of $2.9 M_\odot \text{yr}^{-1}$ (wind scenario B) provided that their cross-section is < 20 kpc in order to match the observed evolution of dN/dz .

Samples with known halo masses such as LBGs (Adelberger et al. 2005) and $z = 1$ Mg II absorbers (Bouché et al. 2006) are shown by the large triangle and circle respectively. As mentioned in section 4.1, the expected SFRs determined by Eq. 2 for these samples agree well with the observed SFRs leading to the conclusion the accretion efficiency ϵ must be high (e.g. Genel et al. 2008). The wind scenario in low mass galaxies is represented by the large filled square (labeled B) in Fig. 4.

4.3.2 Accretion scenario

A third possibility is that Mg II absorbers reside in haloes of intermediate mass with $M_h \sim 10^{10.6-11.0} M_\odot$, i.e. between the two extremes of $10^{10.4} M_\odot$ and $10^{11.3} M_\odot$ already discussed. This mass scale for the $z \sim 2$ hosts is illustrated by the large diamond (labeled A) in Fig. 4. This mass scale falls *below* the grey band in Fig. 4. The grey band illustrates the regime where the accretion efficiency (or cooling efficiency) is certain to be high. This band is defined by a low and high mass. The high mass represents the shock mass $M_{\text{sh}} \sim 10^{12} M_\odot$, the well-known transition between cold and hot accretion (e.g. Birnboim & Dekel 2003; Kereš et al. 2005; Dekel & Birnboim 2006; Kereš et al. 2009; Dekel et al. 2009). The lower mass $M_{\text{min}} \sim 10^{11} M_\odot$ represents another possible transi-

tion⁹ in the cooling properties of haloes (e.g. Cantalupo 2010). This M_{min} hypothesis was postulated in Bouché et al. (2010) because these authors realized a simple analytical model with this single hypothesis could reproduce several key observational results, such as the Tully-Fisher relation, the SFR- M_* sequence, the downsizing phenomenon, the gas fractions (f_g), stellar fractions, and the cosmic star-formation history ($\dot{\rho}_*$).

Since we did not detect the majority of the galaxies, this intermediate mass scale scenario (labeled A in Fig. 4) implies that the efficiency ϵ for accretion in Eq. 2 must be much smaller than our fiducial value of $\epsilon = 1.0$, otherwise the SFRs would have been above our observational limit. Turning it around, the accretion efficiency ϵ should have evolved by about $2.5 \times$ from $10^{10.8} M_\odot$ to $10^{11.3} M_\odot$, i.e. this scenario would imply that $\epsilon(M_h)$ goes as M_h^β with $\beta > 1$. In other words, the mass dependence of ϵ is super-linear. This has the advantage that this scenario can explain both the detections and the non-detections by invoking a finite scatter around a $M_h - W_r^{\lambda 2796}$ relation.

5 ON THE NATURE OF H I-SELECTED ABSORBERS.

As for the Mg II sample, the only criterion used when selecting H I absorbers is the redshift to ensure that the spectral region expected for H α in SINFONI is free of bright sky emission lines. From the samples available in the literature, we observed 7 fields, and detected only one host (see Table 2). We also include the 12 $z = 2$ sight-lines from Péroux et al. (2011b), leading to a total sample of 19 H I-selected absorbers. Admittedly, this H I-selected sample does not cover the whole range of H I columns and metallicities for DLAs, but its mean column density is that of a typical DLA.

In all, out of 19 H I-selected sight-lines, only 2 $z \simeq 2$ hosts have been detected so far with SINFONI. Contrary to the Mg II systems, we cannot give a statistical significance to this result since the $z = 1$ success rate for H I-selected absorbers is poorly constrained. We note that the $z = 1$ success rate for H I-absorbers appears somewhat higher: out of 9 $z = 1$ sight-lines observed with SINFONI, Péroux et al. (2011a) and Péroux et al. (2011b) detected the host towards 4 H I-absorbers.

Thus, our main result for H I-selected absorbers is similar to that of our Mg II-selected sample and to many other $z \sim 2$ DLA surveys, which have also failed to unveil large numbers of hosts using a range of techniques. This is a surprising outcome given that the effort invested and given that sub-DLA/DLAs cover almost the entire sky (e.g. Péroux et al. 2003; Prochaska & Wolfe 2009; Noterdaeme et al. 2009). Among the most sensitive recent studies, there is the stacking analysis of 341 DLAs with $\log N_{\text{HI}}(\text{cm}^{-2}) \gtrsim 20.62$ by Rahmani et al. (2010) who could only place a 3σ upper limit of $3.0 \times 10^{18} \text{erg s}^{-1} \text{cm}^{-2}$ on the average Ly α flux, corresponding to $0.03 L^*(\text{Ly}\alpha)$. There is also the analysis of Wolfe & Chen (2006) who searched for in situ star formation in DLAs by looking for low surface brightness emission in the Hubble Ultra Deep Field (HUDF) F606W image and could also only place upper limits on the SFRs surface density. These upper limits were, surprisingly, at least a factor 10 lower than the rates predicted by the distribution of neutral-gas column densities in DLAs, assuming a normal SF law.

⁹ Note that the power law $\propto M_h^\beta$ index at this transition is directly related to the slope of the luminosity function (see also Kravtsov 2010).

A complete review of recent literature results is beyond the scope of this paper, but in general very few DLA hosts have been identified in spite of numerous search campaigns during the past two decades (e.g. Deharveng et al. 1990; Lowenthal et al. 1990, 1995; Bunker et al. 1995, 1999; Møller et al. 2002; Kulkarni et al. 2000, 2006, among others). Indeed, these efforts led to only 5 bona-fide¹⁰ intervening DLAs which have been identified spectroscopically in emission (Lowenthal et al. 1991; Djorgovski et al. 1996; Möller et al. 2004; Heinmüller et al. 2006; Fynbo et al. 2010). Interestingly, the recent host discovered by Fynbo et al. (2010) towards Q2222-09 meets our Mg II criterion with $W_r^{\lambda 2796} \sim 2.7\text{\AA}$, and has a large SFR of $\sim 17M_\odot \text{ yr}^{-1}$ (uncorrected for dust) from recent SINFONI observations (Péroux et al. 2011b). There is also the one candidate of Fumagalli et al. (2010) who used the ‘Lyman limit’ technique of O’Meara et al. (2006) to image DLA hosts behind a Lyman limit system used as blocking filter.¹¹ Recently, some have argued that a ‘metallicity’ criterion such as $\text{Si II}1526 > 1\text{\AA}$ (e.g. Fynbo et al. 2010) may help in pre-selecting detectable hosts. Evidence for such a metallicity boost is emerging from the survey of Péroux et al. (2011b) where they found, over a wider range of redshift, a 30% success rate for high-metallicity DLAs (with $[\text{Zn}/\text{H}] > -0.65$) versus 10% for the low metallicity sample. In other words, the $z = 2$ detection rate might still be low even for high-metallicity DLAs.

Overall, our low detection rate in conjunction with these literature results are at odds with recent cosmological simulations. Using the state-of-the-art adaptive mesh-refinement (AMR) code ENZO, Cen (2011) found that, in cosmological simulations, DLAs can arise in a wide variety of environments, from cold gas clouds in galactic disks to cold streams to cooling gas from galactic winds to cool clouds entrained by hot galactic winds. However, the prediction at $z = 2$ is that DLAs occur within < 30 kpc of a blue star-forming galaxy, with a SFR of $0.3\text{--}30 M_\odot \text{ yr}^{-1}$, peaking at $6\text{--}8 M_\odot \text{ yr}^{-1}$. The cosmological simulation of Cen (2011) predicts that about two thirds (or 6) of the hosts should meet our survey limits, whereas we detected 2. Pontzen et al. (2008) found that the majority of DLAs reside in halos with $10^{10}M_\odot$ and near galaxies with star formation rates with $> 1M_\odot \text{ yr}^{-1}$. All these models show that DLAs typically arise a few kpc away from galaxies that would be identified in emission with significant SFRs. Our low detection rate—in conjunction with the literature results—disfavors these models.

6 CONCLUSIONS

In summary, we used the SINFONI IFU to search for the H α signature of the hosts towards 18 Mg II absorbers with $W_r^{\lambda 2796} > 2\text{\AA}$. We found the following.

- Only 3 hosts out of our sample of 18 Mg II absorbers with $W_r^{\lambda 2796} \gtrsim 2\text{\AA}$ were detected (Fig. 1) down to impact parameters of $\sim 15\text{--}30$ kpc, reside in haloes with $M_h \sim 2\text{--}3 \times 10^{11}M_\odot$, have dynamical masses $M_{1/2} \sim 2 \times 10^{10}M_\odot$ and SFRs ranging from 9 to $18 M_\odot \text{ yr}^{-1}$;

- Such a low detection rate (4/20)—including two other SINFONI results from Péroux et al. (2011b)—is in sharp contrast to our $z = 1$ SIMPLE survey where we detected 14 out of 21 hosts

(Bouché et al. 2007). Taking into account the difference in sensitivity between the two surveys, we should have been able to detect $\gtrsim 11.4$ ($\gtrsim 7.6$) of the 20 Mg II hosts assuming an evolution of the SFRs as $\propto (1+z)^\gamma$ with $\gamma = 2.5$ ($\gamma = 0$), whereas only 4 were detected. This is statistically significant at the 3.4σ (2.0σ) confidence level, respectively;

- The SFR distribution at $z = 2$ is strikingly different to that at $z = 1$ (Fig. 2). At $z \simeq 2$, all three detections have $\text{SFR} \gtrsim 9 M_\odot \text{ yr}^{-1}$, while at $z = 1$, all the hosts have $\text{SFR} \lesssim 9 M_\odot \text{ yr}^{-1}$. The increase from $z = 1$ to $z = 2$ in the SFRs for the detected hosts is consistent with the evolution of the SFR–mass sequence, which goes as $\propto (1+z)^{2.7}$.

- The undetected $z = 2$ hosts cannot be hidden under the quasar continuum. After stacking our SINFONI cubes, we find no detectable H α emission within $0.3''$ of the QSO to our SFR limit (Fig. 3). Furthermore, the hosts cannot just be outside our surveyed area of $10'' \times 10''$ ($80 \text{ kpc} \times 80 \text{ kpc}$). This would run against our sample selection criteria ($W_r^{\lambda 2796} > 2\text{\AA}$) and the known $W_r^{\lambda 2796}$ –impact parameter relation for low-ionization ions (e.g. Lanzetta & Bowen 1990; Steidel et al. 1995). For instance, the anti-correlation between Si II1526 rest-EW and ρ of Steidel et al. (2010) would place all of our hosts within 40 kpc given that our sample has a mean rest-EW of 0.8\AA in Si II1526.

It is thus very unlikely that they be outside the field of view since this would contradict the recent observations of Steidel et al. (2010).

- We also search for the host galaxy towards 7 H I-selected absorbers, and found only 1 H α emitter. Including the 12 sight-lines from Péroux et al. (2011b), only 2 H I-absorbers out of 19 sight-lines have been detected with SINFONI. This low detection rate (2/19) disfavors the interpretation of Rafelski et al. (2011) that DLAs are probing the outskirts of LBGs.

Our low-detection rate directly imply that the $z = 2$ Mg II hosts cannot reside in haloes with similar masses than those at $z = 1$ which have $M_h \sim 10^{11.3} M_\odot$. Otherwise their SFRs would have been well above our limit. Consequently, strong Mg II systems could reside (i) in haloes with very low masses ($M_h \lesssim 10^{10.6} M_\odot$), or (ii) in haloes with intermediate mass with $M_h \sim 10^{10.8} M_\odot$. The first option (option B in Fig. 4) is consistent with the wind scenario, in which the large equivalent widths are caused by the cold ($T \sim 10^4$ K) material entrained in the super-nova driven outflows generated in very low mass galaxies. Under this scenario, in order to not violate the observed number of absorbers dN/dX , the cross-section of $W_r^{\lambda 2796} > 2\text{\AA}$ -selected winds ought to be ≤ 20 kpc. However, this wind scenario cannot explain the detections and non-detections at the same time since the $W_r^{\lambda 2796}$ -to-SFR ratio must have evolved in opposite directions from $z = 1$ for the two sub-samples.

An alternative option (option A in Fig. 4) is that $z = 2$ Mg II absorbers reside in haloes of intermediate mass with $M_h \sim 10^{10.6\text{--}11.0} M_\odot$. In this case, $z = 2$ galaxies traced by strong Mg II absorbers do not form stars at a rate expected for their halo mass, in contrast to LBGs (and all other SF galaxies) which do form stars at a rate expected for their halo mass provided that the accretion efficiency $\epsilon = 1.0$ is high (e.g. Genel et al. 2008). Since we did not detect the majority of the galaxies, this scenario implies that the efficiency ϵ for accretion is much smaller at those mass scales otherwise the SFRs would have been above our observational limit. In other words, this would support the existence of a transition in accretion (and/or galaxy properties) at $M_h \sim 10^{11} M_\odot$, where

¹⁰ Excluding the proximate $z_{\text{qso}} \simeq z_{\text{dla}}$ DLAs.

¹¹ The disadvantage of this technique, which relies on broad-band imaging, is that only candidates can be found.

cooling is less efficient in low mass haloes. This scenario implies that $\epsilon(M_h)$ goes as M_h^β with $\beta > 1$. A consequence of this steep mass-dependence is that this scenario can explain both the detections and the non-detections by invoking a finite scatter around a $M_h - W_r^{\lambda 2796}$ relation.

Clearly, some star-formation must have occurred in the past to produce these metals. The very nature of Mg II systems means that SF occurred and enriched these regions (with α -elements) at an earlier epoch. This pre-enrichment scenario is supported by the recent analysis of the clustering of C IV systems by Martin et al. (2010), where they found that the size of enriched regions around $z = 2$ to $z = 4.5$ galaxies is large ~ 0.4 Mpc (co-moving). The implied time scale for dispersing metals to such distances is larger than the typical stellar ages of SF galaxies. This means that enrichment by (low-mass) galaxies at an earlier epoch $z > 4.5$ must have occurred to account for the metal enriched regions traced by strong Mg II intervening absorbers.

7 ACKNOWLEDGMENTS

We thank Kyle Stewart and Shy Genel for discussions. We thank the ESO staff for their support in carrying these observations and take the opportunity to thank the entire SINFONI instrument team. We thank the anonymous referee for a constructive and detailed report that led to significant improvements of the draft. This research was supported by a Marie Curie International Outgoing Fellowship (PIOF-GA-2009-236012) within the 7th European Community Framework Programme. MTM thanks the Australian Research Council for a QEII Research Fellowship (DP0877998). We acknowledge the use of the Sloan Digital Sky Survey (SDSS). Funding for the SDSS and SDSSII has been provided by the Alfred P. Sloan Foundation, the Participating Institutions, the National Science Foundation, the U.S. Department of Energy, the National Aeronautics and Space Administration, the Japanese Monbukagakusho, the Max Planck Society, and the Higher Education Funding Council for England.

REFERENCES

- Abazajian, K., & et al., 2003, *AJ*, 126, 2081
 Abazajian, K. N. et al. 2009, *ApJS*, 182, 543
 Abuter, R., Schreiber, J., Eisenhauer, F., Ott, T., Horrobin, M., & Gillesen, S. 2006, *New Astronomy Review*, 50, 398
 Adelberger, K. L., Steidel, C. C., Pettini, M., Shapley, A. E., Reddy, N. A., & Erb, D. K. 2005, *ApJ*, 619, 697
 Behroozi, P. S., Conroy, C., & Wechsler, R. H. 2010, *ApJ*, 717, 379
 Bergeron, J., & Boissé, P. 1991, *A&A*, 243, 344
 Bergeron, J., Cristiani, S., & Shaver, P. A. 1992, *A&A*, 257, 417
 Birnboim, Y., & Dekel, A. 2003, *MNRAS*, 345, 349
 Birnboim, Y., Dekel, A., & Neistein, E. 2007, *MNRAS*, 380, 339
 Bond, N. A., Churchill, C. W., Charlton, J. C., & Vogt, S. S. 2001, *ApJ*, 557, 761
 Bonnet, H. et al. 2004, in Presented at the Society of Photo-Optical Instrumentation Engineers (SPIE) Conference, Vol. 5490, Society of Photo-Optical Instrumentation Engineers (SPIE) Conference Series, ed. D. Bonaccini Calia, B. L. Ellerbroek, & R. Ragazzoni, 130–138
 Bouché, N. et al. 2010, *ApJ*, 718, 1001
 Bouché, N., Murphy, M. T., Péroux, C., Csabai, I., & Wild, V. 2006, *MNRAS*, 371, 495
 Bouché, N., Murphy, M. T., Péroux, C., Davies, R., Eisenhauer, F., Förster Schreiber, N. M., & Tacconi, L. 2007, *ApJ*, 669, L5
 Budavári, T., & et al., 2003, *ApJ*, 595, 59
 Bunker, A. J., Warren, S. J., Clements, D. L., Williger, G. M., & Hewett, P. C. 1999, *MNRAS*, 309, 875
 Bunker, A. J., Warren, S. J., Hewett, P. C., & Clements, D. L. 1995, *MNRAS*, 273, 513
 Cameron, E. 2011, *Publ. Astron. Soc. Austral.*, 28, 128
 Cantalupo, S. 2010, *MNRAS*, 403, L16
 Cen, R. 2011, *ApJ*, submitted
 Chabrier, G. 2003, *PASP*, 115, 763
 Chen, H., Wild, V., Tinker, J. L., Gauthier, J., Helsby, J. E., Shectman, S. A., & Thompson, I. B. 2010, *ApJ*, 724, L176
 Churchill, C. W., Mellon, R. R., Charlton, J. C., Jannuzi, B. T., Kirhakos, S., Steidel, C. C., & Schneider, D. P. 2000, *ApJS*, 130, 91
 Daddi, E. et al. 2007, *ApJ*, 670, 156
 Dahlen, T., Mobasher, B., Dickinson, M., Ferguson, H. C., Giavalisco, M., Kretchmer, C., & Ravindranath, S. 2007, *ApJ*, 654, 172
 Damen, M., Labbé, I., Franx, M., van Dokkum, P. G., Taylor, E. N., & Gawiser, E. J. 2009, *ApJ*, 690, 937
 Davies, R. 2007, *MNRAS*, 375, 1099
 Deharveng, J. M., Buat, V., & Bowyer, S. 1990, *A&A*, 236, 351
 Dekel, A., & Birnboim, Y. 2006, *MNRAS*, 368, 2
 Dekel, A. et al. 2009, *Nat*, 457, 451
 Djorgovski, S. G., Pahre, M. A., Bechtold, J., & Elston, R. 1996, *Nat*, 382, 234
 Drory, N., & Alvarez, M. 2008, *ApJ*, 680, 41
 Dutton, A. A., van den Bosch, F. C., & Dekel, A. 2010, *MNRAS*, 405, 1690
 Eisenhauer, F., & et al. 2003, in *Instrument Design and Performance for Optical/Infrared Ground-based Telescopes*. Edited by Iye, Masanori; Moorwood, Alan F. M. Proceedings of the SPIE, Volume 4841, pp. 1548-1561 (2003), ed. M. Iye & A. F. M. Moorwood, 1548–1561
 Eisenstein, D. J., & et al., 2005, *ApJ*, 633, 560
 Elbaz, D. et al. 2007, *A&A*, 468, 33
 Ellison, S. L. 2006, *MNRAS*, 368, 335
 Erb, D. K., Steidel, C. C., Shapley, A. E., Pettini, M., Reddy, N. A., & Adelberger, K. L. 2006, *ApJ*, 647, 128
 Faucher-Giguère, C.-A., & Kereš, D. 2011, *MNRAS*, 412, L118
 Förster Schreiber, N. M. et al. 2009, *ApJ*, 706, 1364
 —. 2006, *ApJ*, 645, 1062
 Fumagalli, M., O’Meara, J. M., Prochaska, J. X., & Kanekar, N. 2010, *MNRAS*, 408, 362
 Fynbo, J. P. U. et al. 2010, *MNRAS*, 408, 2128
 —. 2011, *MNRAS*, 413, 2481
 Gauthier, J., Chen, H., & Tinker, J. L. 2009, *ApJ*, 702, 50
 Genel, S. et al. 2008, *ApJ*, 688, 789
 Guo, Q., White, S., Li, C., & Boylan-Kolchin, M. 2010, *MNRAS*, 404, 1111
 Heinmüller, J., Petitjean, P., Ledoux, C., Caucci, S., & Srianand, R. 2006, *A&A*, 449, 33
 Kacprzak, G. G., Churchill, C. W., Ceverino, D., Steidel, C. C., Klypin, A., & Murphy, M. T. 2010, *ApJ*, 711, 533
 Karim, A. et al. 2011, *ApJ*, 730, 61
 Kereš, D., Katz, N., Fardal, M., Dave, R., & Weinberg, D. H. 2009, *MNRAS*, 395, 160

- Kereš, D., Katz, N., Weinberg, D. H., & Davé, R. 2005, *MNRAS*, 363, 2
- Kimm, T., Slyz, A., Devriendt, J., & Pichon, C. 2011, *MNRAS*, 413, L51
- Kravtsov, A. V. 2010, *Advances in Astronomy*, 2010
- Kulkarni, V. P., Hill, J. M., Schneider, G., Weymann, R. J., Storrie-Lombardi, L. J., Rieke, M. J., Thompson, R. I., & Jannuzi, B. T. 2000, *ApJ*, 536, 36
- Kulkarni, V. P., Woodgate, B. E., York, D. G., Thatte, D. G., Meiring, J., Palunas, P., & Wassell, E. 2006, *ApJ*, 636, 30
- Lanzetta, K. M., & Bowen, D. 1990, *ApJ*, 357, 321
- Larson, R. B. 1974, *MNRAS*, 166, 585
- Ledoux, C., Petitjean, P., Fynbo, J. P. U., Møller, P., & Srianand, R. 2006, *A&A*, 457, 71
- Lopez, S., Reimers, D., D’Odorico, S., & Prochaska, J. X. 2002, *A&A*, 385, 778
- Lowenthal, J. D., Hogan, C. J., Green, R. F., Caulet, A., Woodgate, B. E., Brown, L., & Foltz, C. B. 1991, *ApJ*, 377, L73
- Lowenthal, J. D., Hogan, C. J., Green, R. F., Woodgate, B., Caulet, A., Brown, L., & Bechtold, J. 1995, *ApJ*, 451, 484
- Lowenthal, J. D., Hogan, C. J., Leach, R. W., Schmidt, G. D., & Foltz, C. B. 1990, *ApJ*, 357, 3
- Lundgren, B. F. et al. 2009, *ApJ*, 698, 819
- Madgwick, D. S., & et al., 2003, *MNRAS*, 344, 847
- Martin, C. L., & Bouché, N. 2009, *ApJ*, 703, 1394
- Martin, C. L., Scannapieco, E., Ellison, S. L., Hennawi, J. F., Djorgovski, S. G., & Fournier, A. P. 2010, *ApJ*, 721, 174
- McBride, J., Fakhouri, O., & Ma, C. 2009, *MNRAS*, 398, 1858
- Ménard, B., Wild, V., Nestor, D., Quider, A., & Zibetti, S. 2011, *MNRAS*, submitted
- Mo, H. J., & White, S. D. M. 2002, *MNRAS*, 336, 112
- Möller, P., Fynbo, J. P. U., & Fall, S. M. 2004, *A&A*, 422, L33
- Møller, P., Warren, S. J., Fall, S. M., Fynbo, J. U., & Jakobsen, P. 2002, *ApJ*, 574, 51
- Mosleh, M., Williams, R. J., Franx, M., & Kriek, M. 2011, *ApJ*, 727, 5
- Moster, B. P., Somerville, R. S., Maulbetsch, C., van den Bosch, F. C., Macciò, A. V., Naab, T., & Oser, L. 2010, *ApJ*, 710, 903
- Murphy, M. T., & Liske, J. 2004, *MNRAS*, 354, L31
- Neistein, E., & Dekel, A. 2008, *MNRAS*, 388, 1792
- Neistein, E., van den Bosch, F. C., & Dekel, A. 2006, *MNRAS*, 372, 933
- Nestor, D. B., Johnson, B. D., Wild, V., Ménard, B., Turnshek, D. A., Rao, S., & Pettini, M. 2011, *MNRAS*, 412, 1559
- Nestor, D. B., Turnshek, D. A., & Rao, S. M. 2005, *ApJ*, 628, 637
- Noterdaeme, P., Petitjean, P., Ledoux, C., & Srianand, R. 2009, *A&A*, 505, 1087
- Noterdaeme, P., Srianand, R., & Mohan, V. 2010, *MNRAS*, 403, 906
- Nulsen, P. E. J., Barcons, X., & Fabian, A. C. 1998, *MNRAS*, 301, 168
- Ocvirk, P., Pichon, C., & Teyssier, R. 2008, *MNRAS*, 390, 1326
- O’Meara, J. M., Chen, H., & Kaplan, D. L. 2006, *ApJ*, 642, L9
- Péroux, C., McMahon, R. G., Storrie-Lombardi, L. J., & Irwin, M. J. 2003, *MNRAS*, 346, 1103
- Pannella, M. et al. 2009, *ApJ*, 698, L116
- Péroux, C., Bouché, N., Kulkarni, V. P., York, D. G., & Vladilo, G. 2011a, *MNRAS*, 410, 2237
- Péroux, C., Kulkarni, V. P., York, D. G., Vladilo, G., & Bouché, N. 2011b, *MNRAS*, submitted.
- Pontzen, A. et al. 2008, *MNRAS*, 390, 1349
- Prochaska, J. X., Herbert-Fort, S., & Wolfe, A. M. 2005, *ApJ*, 635, 123
- Prochaska, J. X., & Wolfe, A. M. 1997, *ApJ*, 487, 73
- . 2009, *ApJ*, 696, 1543
- Prochter, G. E., Prochaska, J. X., & Burles, S. 2006, *ApJ*, 639, 766
- Rafelski, M., Wolfe, A. M., & Chen, H.-W. 2011, *ApJ*, 736, 48
- Rahmani, H., Srianand, R., Noterdaeme, P., & Petitjean, P. 2010, *MNRAS*, 409, L59
- Rao, S. M., Turnshek, D. A., & Nestor, D. B. 2006, *ApJ*, 636, 610
- Reimers, D., & Wisotzki, L. 1997, *The Messenger*, 88, 14
- Rubin, K. H. R., Weiner, B. J., Koo, D. C., Martin, C. L., Prochaska, J. X., Coil, A. L., & Newman, J. A. 2010, *ApJ*, 719, 1503
- Ryabinkov, A. I., Kaminker, A. D., & Varshalovich, D. A. 2003, *A&A*, 412, 707
- Santini, P. et al. 2009, *A&A*, 504, 751
- Schaye, J. 2001, *ApJ*, 559, L1
- Schmidt, M. 1963, *ApJ*, 137, 758
- Schreiber, J., Thatte, N., Eisenhauer, F., Tecza, M., Abuter, R., & Horrobin, M. 2004, in *ASP Conf. Ser. 314: Astronomical Data Analysis Software and Systems (ADASS) XIII*, ed. F. Ochsenbein, M. G. Allen, & D. Egret, 380–+
- Shankar, F., Lapi, A., Salucci, P., De Zotti, G., & Danese, L. 2006, *ApJ*, 643, 14
- Springel, V., Frenk, C. S., & White, S. D. M. 2006, *Nat*, 440, 1137
- Srianand, R., Noterdaeme, P., Ledoux, C., & Petitjean, P. 2008, *A&A*, 482, L39
- Steidel, C. C. 1995, in *QSO Absorption Lines*, ed. G. Meylan, *ESO Astrophysics Symposia (Berlin, Germany: Springer-Verlag)*, 139
- Steidel, C. C., Bowen, D. V., Blades, J. C., & Dickinson, M. 1995, *ApJ*, 440, L45
- Steidel, C. C., Erb, D. K., Shapley, A. E., Pettini, M., Reddy, N., Bogosavljević, M., Rudie, G. C., & Rakic, O. 2010, *ApJ*, 717, 289
- Steidel, C. C., & Sargent, W. L. W. 1992, *ApJS*, 80, 1
- Stewart, K. R., Kaufmann, T., Bullock, J. S., Barton, E. J., Maller, A. H., Diemand, J., & Wadsley, J. 2011, *ApJ*, 735, L1+
- Tinker, J. L., & Chen, H.-W. 2008, *ApJ*, 679, 1218
- van de Voort, F., Schaye, J., Booth, C. M., Haas, M. R., & Dalla Vecchia, C. 2011, *MNRAS*, 414, 2458
- van den Bergh, S. 1962, *AJ*, 67, 486
- van den Bosch, F. C. et al. 2007, *MNRAS*, 376, 841
- van Dokkum, P. G. 2001, *PASP*, 113, 1420
- Weiner, B. J. et al. 2009, *ApJ*, 692, 187
- White, S. D. M., & Frenk, C. S. 1991, *ApJ*, 379, 52
- White, S. D. M., & Rees, M. J. 1978, *MNRAS*, 183, 341
- Williams, R. J., Quadri, R. F., Franx, M., van Dokkum, P., Toft, S., Kriek, M., & Labbé, I. 2010, *ApJ*, 713, 738
- Wolfe, A. M., & Chen, H.-W. 2006, *ApJ*, 652, 981
- Zibetti, S., Ménard, B., Nestor, D. B., Quider, A. M., Rao, S. M., & Turnshek, D. A. 2007, *ApJ*, 658, 161

This paper has been typeset from a $\text{\TeX}/\text{\LaTeX}$ file prepared by the author.

Table 1. Summary of new observations.

QSO (1)	z_{qso} (2)	z_{abs} (3)	$W_r(\text{Å})$ (4)	Ref. (5)	PSF(") (6)	$t_{\text{exp}}(\text{s})$ (7)	Run ID (8)	Dates (9)
Mg II-selected								
SDSSJ031522.09-080043.7	2.8940	2.06056	2.9/2.9	(1)	0.7	3000	076.A-0527	2005-10-07
SDSSJ091247.59-004717.3	2.8590	2.07097	2.3/2.2	(1)	0.6	2400	076.A-0527	2006-03-18
SDSSJ103446.54+110214.4	4.2660	2.11605	2.9/1.8	(1)	0.6	4800	081.A-0682	2008-03-31
SDSSJ104252.32+011736.5	2.440	2.2667	2.3/2.2	(1)	0.6	4800	081.A-0682	2008-03-30
SDSSJ104747.08+045638.6	2.1220	2.07129	2.8/2.3	(1)	0.6	2400	076.A-0527	2006-03-18
SDSSJ111008.61+024458.0	4.1170	2.11874	2.6/2.9	(1)	0.6	12000	081.A-0682 082.A-0580	2008-03-31 2009-01-10
SDSSJ114436.65+095904.9	3.1500	2.09277	4.1/3.3	(1)	0.6	4800	081.A-0682	2008-04-02
J1205-0742	4.694	2.44400	3.9/2.8	(1)	0.6	4800	081.A-0682	2008-04-21
SDSSJ125525.67+030518.4	2.5300	2.11441	3.2/2.9	(1)	0.5	4800	082.A-0580	2009-02-29
SDSSJ130907.93+025432.6	2.9400	2.24588	2.1/1.1	(1)	0.7	4800	082.A-0580	2009-01-22 2009-02-07
SDSSJ131625.40+124411.8	3.0940	2.03673	3.4/2.0	(1)	0.7	2400	079.A-0341	2007-03-19
SDSSJ132139.86-004151.9	3.0740	2.22157	3.7/2.5	(1)	0.6	4800	081.A-0682	2008-04-23
SDSSJ143500.27+035403.5	2.4920	2.27065	2.6/2.3	(1)	0.9	2400	079.A-0600	2007-04-19
SDSSJ151824.37-010149.8	2.5860	2.03632	2.0/2.1	(1)	0.5	4800	082.A-0580	2009-02-28
SDSSJ161526.64+264813.7	2.1800	2.11728	4.4/4.3	(1)	0.6	4800	081.A-0682	2008-04-02
SDSSJ205724.14-003018.7	4.6630	2.26871	2.2/2.2	(1)	0.7	4800	081.A-0682	2008-10-04
Q2243-60 ¹	3.01	2.3288	2.6	(2)	0.75	9600	060.A-9041	2004-08-17/19
SDSSJ233156.47-090802.0	2.6610	2.14265	1.9/2.6	(1)	0.8	2400	076.A-0527	2005-10-08
H I-selected			$\log N_{\text{HI}}$					
SDSSJ004732.73+002111.3	2.8788	2.4687	20.0	(3)	0.6	6000	081.A-0682	2008-09-15
SDSSJ013317.79+144300.3	3.2323	2.4754	20.0	(3)	0.6	4800	081.A-0682	2008-09-15
Q0216+080	2.99	2.2931	20.50	(4)	0.8	9600	060.A-9041	2004-08-14/15
Q1037-27	2.19	2.13900	19.70	(5)	0.6	2400	079.A-0341	2007-04-18
SDSSJ131757.98+055938.6	2.3111	2.1742	20.05	(3)	0.6	1200	081.A-0682	2008-04-15
SDSSJ143912.04+111740.5	2.5827	2.4184	20.25	(6)	1.0	2400	081.A-0568	2008-04-09
Q2243-60 ¹	3.01	2.3288	20.67	(2)	0.75	9600	060.A-9041	2004-08-17/19

(1) QSO name; (2) QSO emission redshift; (3) Absorber redshift; (4) Mg II rest-equivalent width (Å) / $\log N_{\text{HI}}(\text{cm}^{-2})$; (5) References for W_r or $\log N_{\text{HI}}$ (1: This work; 2: From Lopez et al. (2002); 3: From Prochaska et al. (2005); 4: From Ledoux et al. (2006) 5: From Ryabinkov et al. (2003); 6: From Srianand et al. (2008)); (6) FWHM of the seeing PSF; (7) Exposure time; (8) Observing run ID; (9) Dates of observations.

¹Source common to both samples.

Table 2. Combined Sample Properties.

Sight Line (1)	z_{qso} (2)	z_{abs} (3)	$W_r(\text{\AA})$ (4)	$\log N_{\text{HI}}$ (5)	$5\sigma_{\text{H}\alpha}$ (6)	$5\sigma_{\text{SFR}}$ (7)	$\Delta_{RA}, \Delta_{Dec}$ (8)	ρ (9)	$f_{\text{H}\alpha}$ (10)	SFR (11)	SFR ₀ (12)	Ref. (13)
Mg II-selected						< 1.8	< 2.9					
SDSSJ031522.09-080043.7	2.8940	2.06056	2.9/2.9	0	< 2.8	< 4.0	(1)
SDSSJ091247.59-004717.3	2.8590	2.07097	2.3/2.2	0	< 4.0	< 7.3	(1)
SDSSJ103446.54+110214.4	4.2660	2.11605	2.9/1.8	0	< 1.3	< 2.0	(1)
SDSSJ104252.32+011736.5	2.440	2.2667	2.3/2.2	...	< 1.0	< 1.7	(1)
SDSSJ104747.08+045638.6	2.1220	2.07129	2.8/2.3	0	< 4.0	< 7.2	(1)
SDSSJ111008.61+024458.0	4.1170	2.11874	2.6/2.9	1	< 0.8	< 1.2	+2.0,-0.25	16.6	6.0	9.1	19.2	(1)
SDSSJ114436.65+095904.9	3.1500	2.09277	4.1/3.3	1	< 1.2	< 1.5	(+1.2,+1.85)	(18.6) ⁴	(1)
J1205-0742	4.694	2.44400	3.9/2.8	0	< 1.6	< 3.5	(1)
SDSSJ125525.67+030518.4	2.5300	2.11441	3.2/2.9	1	< 0.9	< 1.4	+1.125,-1.25 +4.00,+2.37	14.1 38.7	5.6 7.1	8.6 10.8	18.0 22.6	(1)
SDSSJ130907.93+025432.6	2.9400	2.24588	2.1/1.1	0	< 1.2	< 2.1	(1)
SDSSJ131625.40+124411.8	3.0940	2.03673	3.4/2.0	0	< 4.0	< 5.6	(1)
SDSSJ132139.86-004151.9	3.0740	2.22157	3.7/2.5	0	< 1.2	< 2.1	(1)
SDSSJ143500.27+035403.5	2.4920	2.27065	2.6/2.3	1	< 1.8	< 3.0	(1)
SDSSJ151824.37-010149.8	2.5860	2.03632	2.0/2.1	1	< 1.2	< 1.7	(1)
SDSSJ161526.64+264813.7	2.1800	2.11728	4.4/4.3	0	< 1.1	< 1.7	(1)
SDSSJ205724.14-003018.7	4.6630	2.26871	2.2/2.2	0	< 1.2	< 2.2	(1)
Q2243-60	3.01	2.3288	2.6 ²	20.67	< 0.6	< 1.3	-2.1,-2.1	26.5	8.0	17	36	(1)
SDSSJ233156.47-090802.0	2.6610	2.14265	1.9/2.6	1	< 2.4	< 3.6	(1)
SDSSJ205922.42-052842.7 ¹	2.539	2.2100	2.1/1.7	20.80	< 1.6	< 2.7	(2)
SDSSJ222256.11-094636.2 ¹	2.927	2.3543	2.7 ³	20.50	< 1.1	< 2.2	+0.5,+0.5	6	9.0	18	37	(2)
H I-selected						< 5						
SDSSJ004732.73+002111.3	2.8788	2.4687	...	20.00	< 2.1	< 4.9	(1)
SDSSJ013317.79+144300.3	3.2323	2.4754	...	20.00	< 1.9	< 4.3	(1)
Q0216+080	2.99	2.29	...	20.50	< 1.0	< 1.8	(1)
Q1037-27	2.19	2.13900	...	19.70	< 3.0	< 4.7	(1)
SDSSJ131757.98+055938.6	2.3111	2.1742	1.6/1.3	20.05	< 2.4	< 4.3	(1)
SDSSJ143912.04+111740.5	2.5827	2.4184	...	20.25	< 2.3	< 3.9	(1)
Q2243-60	3.01	2.3288	2.6 ²	20.67	< 0.8	< 1.5	-2.1,-2.1	26.5	8.0	17	36	(1)
SDSSJ121134.95+090220.8	3.292	2.5841	...	21.40	< 5.6	< 14	(2)
SDSSJ122607.19+173649.8	2.925	2.5576	...	19.32	< 6.8	< 17	(2)
Q1228-113	3.528	2.1929	...	20.60	< 0.8	< 1.4	(2)
Q1232+07	2.570	2.3376	...	20.80	< 0.8	< 1.6	(2)
Q1354-11	3.006	2.5009	...	20.40	< 2.2	< 5.2	(2)
SDSSJ145418.58+121053.8	3.256	2.2550	1.0/0.9	20.30	< 2.1	< 3.7	(2)
SDSSJ205922.42-052842.7 ¹	2.539	2.2100	2.1/1.6	20.80	< 1.6	< 2.7	(2)
Q2102-35	3.090	2.5070	...	20.21	< 3.1	< 7.2	(2)
SDSSJ222256.11-094636.2 ¹	2.927	2.3543	2.7 ³	20.50	< 1.1	< 2.2	+0.5,+0.5	6	9.0	18	37	(2)
Q2311-37	2.476	2.1821	...	20.48	< 1.5	< 2.5	(2)
SDSSJ235057.87-005209.9	3.023	2.6147	...	21.30	< 4.0	< 10	(2)
Q2359-01	2.810	2.0950	...	20.70	< 1.3	< 2.0	(2)

(1) Name of QSO sight-line; (2) QSO redshift; (3) Absorber redshift; (4) rest-frame $W_r^{\lambda 2796}/W_r^{2803}$; (5) H I column density or '0/1' indicating whether the system meets the Rao et al. (2006) criteria for being a DLA; (6) H α flux limit (5σ) in $10^{-17} \text{ erg s}^{-1} \text{ cm}^{-2}$; (7) SFR limit (5σ) in $M_{\odot} \text{ yr}^{-1}$ for a Chabrier IMF; (8) R.A., Decl. offsets in $''$; (9) impact parameter in kpc; (10) H α line flux in $10^{-17} \text{ erg s}^{-1} \text{ cm}^{-2}$; (11) observed SFR in $M_{\odot} \text{ yr}^{-1}$ (Chabrier); (12) intrinsic SFR in $M_{\odot} \text{ yr}^{-1}$ corrected for dust; (13) References (1: This work, 2: From the survey of Péroux et al. (2011b)).

¹Source common to both the Mg II and H I sample; ²From Lopez et al. (2002); ³From Fynbo et al. (2010); ⁴Continuum of a source detected with no redshift identification.

Table 3. Sample Results

Sample (1)	N (2)	SFRlimit (3)	\hat{p} (4)	N_e (5)	N_d (6)	P -value(N_d) (7)	SFR(z) (8)
Mg II	20	2.9	8/21	7.6	4	0.045(2.0σ)	no Evol.
Mg II	20	2.9	12/21	11.4	4	0.0007 (3.4σ)	$\propto (1+z)^{2.5}$

(1) Sample name; (2) Number of sight-lines; (3) SFR limit (3σ) in $M_{\odot} \text{ yr}^{-1}$; (4) Success rate expected from the z1SIMPLE results and corrected for the SFR limit; (5) Number of detections expected; (6) Number of actual detections; (7) Probability that exactly N_d -detections occur by chance given the expected success rate \hat{p} ; (8) Assumed evolution of SFR(z).